



System Identification of UCSD-NHERI Shake-Table Test of Two-Story Structure with Cross-Laminated Timber Rocking Walls

Ignace Mugabo, Ph.D.¹; Andre R. Barbosa, Ph.D., P.E., A.M.ASCE²; Arijit Sinha, Ph.D., A.M.ASCE³; Christopher Higgins, Ph.D., P.E., M.ASCE⁴; Mariapaola Riggio, Ph.D.⁵; Shiling Pei, Ph.D., M.ASCE⁶; John W. van de Lindt, Ph.D., F.ASCE⁷; and Jeffrey W. Berman, Ph.D., A.M.ASCE⁸

Abstract: A full-scale 2-story mass timber building was tested on the University of California San Diego Natural Hazards Engineering Research Infrastructure (UCSD-NHERI) uniaxial shake table during the period from June 2017 to September 2017. The main objective of the experimental program was to test the performance of mass timber building designs with different seismic lateral force-resisting systems. The focus of this study is on a building configuration designed using self-centering post-tensioned cross-laminated timber (CLT) rocking walls with U-shaped steel flexural plate energy dissipators. The shake-table tests were designed to subject the building to a series of earthquake ground motions of increasing intensity, ranging from a service-level earthquake to 1.20 times the maximum considered earthquake intensity. Between each ground motion, low-amplitude white-noise excitations were applied to the building, which responded as a quasilinear system. In this paper, two output-only operational modal analysis methods are used to estimate the modal parameters (frequency, damping, and mode shapes) based on acceleration data collected during the white-noise shake-table tests. The correlations of observed damage and repairs performed during the experimental program with changes in estimated modal features are reported. The modal parameters estimated from the testing program are also compared with a linear finite-element model that is used to validate the modal identification results and study the performance of the two system identification methods for CLT rocking structures. DOI: 10.1061/(ASCE)ST.1943-541X.0002938. © 2021 American Society of Civil Engineers.

Introduction

The emerging use of cross-laminated timber (CLT) in the US and across the world is mainly attributed to its stakeholder interest, multidirectional load-carrying capacity, speed of construction,

¹Graduate Research Assistant, School of Civil and Construction Engineering, Oregon State Univ., Corvallis, OR 97331; Structural Engineer, KPFF Consulting Engineers, 111 SW 5th Ave., Suite 2600, Portland, OR 97204. Email: ignace.mugabo@kpff.com

²Associate Professor, School of Civil and Construction Engineering, Oregon State Univ., Corvallis, OR 97331 (corresponding author). ORCID: https://orcid.org/0000-0003-4547-531X. Email: andre.barbosa@oregonstate .edu

³Associate Professor, Dept. of Wood Science and Engineering, Oregon State Univ., Corvallis, OR 97331. ORCID: https://orcid.org/0000-0003 -3718-5910. Email: arijit.sinha@oregonstate.edu

⁴Cecil and Sally Drinkward Professor, School of Civil and Construction Engineering, Oregon State Univ., Corvallis, OR 97331. Email: chris.higgins@oregonstate.edu

⁵Associate Professor, Dept. of Wood Science and Engineering, Oregon State Univ., Corvallis, OR 97331. Email: mariapaola.riggio@oregonstate.edu

⁶Associate Professor, Dept. of Civil and Environmental Engineering, Colorado School of Mines, Golden, CO 80401. Email: spei@mines.edu

⁷Professor, Dept. of Civil and Environmental Engineering, Colorado State Univ., Fort Collins, CO 80523. Email: jwv@engr.colostate.edu

⁸Professor, Dept. of Civil and Environmental Engineering, Univ. of Washington, Seattle, WA 98195. Email: jwberman@uw.edu

Note. This manuscript was submitted on May 18, 2020; approved on October 8, 2020; published online on January 23, 2021. Discussion period open until June 23, 2021; separate discussions must be submitted for individual papers. This paper is part of the *Journal of Structural Engineering*, © ASCE, ISSN 0733-9445.

sustainability, and aesthetics. As an engineered wood product, CLT and other mass timber panels have been recognized as the natural choice for buildings with enhanced sustainability goals because they are made from renewable resources and have less embodied energy (Milaj et al. 2017). With the use of CLT continuing to grow in seismic-prone regions, evaluation of the seismic performance of CLT structural systems is of increased importance (Pei et al. 2016).

Several experimental programs have been developed in the last 2 decades to study the seismic performance of CLT wall systems. In terms of structural performance assessment and design, the most relevant research efforts in Europe and North America have focused on the performance of floor and wall panels and connections for the lateral force-resisting systems (Ceccotti et al. 2006; Dujic et al. 2010; Popovski et al. 2010; van de Lindt et al. 2010; Ceccotti et al. 2013; Iqbal et al. 2015; Sustersic et al. 2016; Ganey et al. 2017; Tannert et al. 2018; Zimmerman and McDonnell 2018; Chen and Popovski 2020a, b; Chen et al. 2020). The Construction System Fiemme (SOFIE) project (Ceccotti et al. 2006) was one of the first comprehensive experimental programs performed to evaluate the lateral resistance and behavior of CLT walls. The SOFIE project comprised element-level monotonic and cyclic tests of full-size CLT walls, a 3-story shake-table test, and a full-scale 7-story CLT structure test performed at the E-Defense shake table in Japan.

The project included the design and shake-table testing of 3-story and 7-story CLT shake-table test specimens. For the 3-story CLT structure (Ceccotti and Follesa 2006), the unidirectional [one-dimensional (1D)] shaking tests included subjecting the structure to 26 earthquake simulated ground motions, which progressively increased the peak ground accelerations (PGA) from 0.15g to 1.20g. Natural frequency reductions due to the more severe

earthquakes (0.5g-1.2g) were all 12% or less, where by design, and even under such intense shaking, the structure exhibited repairable damage.

For the 7-story shake-table test (Ceccotti et al. 2013), the structure was subjected to a total of 10 earthquake motions, including (1) a set of five unidirectional shake-table motions, and (2) five tridirectional shake-table motions. Results from the application of the shake-table motions indicated that the *X*- and *Y*-directions, fundamental frequencies of the 7-story structure exhibited a 24% and 17% reduction from the initial values, respectively. Overall, the 7-story CLT structure produced ductile and self-centering behavior marked with fastener ductile bending failure and embedment failure of the connections at the wall ends. To date, no journal papers were found in the literature that focused on studying modal features and damage propagation of self-centering CLT structures under shake-table experiments.

Self-centering rocking wall systems exhibit rocking deformation behavior under lateral loading. At the same time, post-tensioned tendons are used to recenter the walls to their original position. The conceptual basis behind rocking wall systems is the use of a recentering mechanism, e.g., post-tensioned tendons, coupled with external energy dissipators (e.g., mild steel bars) that are designed to dissipate seismic energy. The rocking wall concept originated from research in precast concrete (Priestley 1991; Holden et al. 2003; Restrepo and Rahman 2007; Belleri et al. 2014; Kurama et al. 2018) and was successfully adapted to timber systems over the last 15 years (e.g., Granello et al. 2020). Post-tensioned timber systems have been detailed in a series of subassembly experiments performed on beam-to-column, column-to-foundation, and wall-tofoundation energy-dissipation solutions using laminated-veneer lumber (LVL) members (Palermo et al. 2005, 2006a, b; Smith et al. 2007) and glued-laminated timber (glulam) members (e.g., Granello et al. 2019). Out of the energy-dissipation methods tested with LVL shear walls by Palermo et al. (2005, 2006a, b) and Smith et al. (2007), the U-shaped flexural plates (UFP) were observed to be the most effective (Smith et al. 2008).

Baird et al. (2014) derived formulas for the yielding force, initial stiffness, and hardening parameter using previous analytical derivations by Kelly et al. (1972), based on experimental tests and finite-element modeling. Kramer et al. (2015) evaluated the tension and cyclic performance of an external energy-dissipation connector to be used on self-centering rocking CLT walls. The results indicated no damage on the CLT members, low variability, and predictable behavior of the energy dissipators. A series of other studies focused on the seismic performance of self-centering CLT walls with UFP devices (Akbas et al. 2017; Ganey et al. 2017).

In 2017, a series of tests were performed in the University of California San Diego Natural Hazards Engineering Research Infrastructure (UCSD-NHERI) shake table for mass timber structures. Testing performed provided benchmark data on the performance of three lateral resisting systems. Thus, the testing was divided into three phases: (1) a self-centering rocking wall design (Pei et al. 2019a), (2) a non-post-tensioned rocking wall design (Blomgren et al. 2019), and (3) a platform-type CLT wall system (van de Lindt et al. 2019). The three studies cited summarize the experimental testing program, including design, as well as the main results obtained for the lateral load-resisting systems. However, a detailed analysis of system identification results had not yet been performed and is developed in this study.

Based on the literature review and existing knowledge, only a limited number of tests on rocking timber systems have been performed on shake tables. No self-centering CLT systems have been tested on a shake table at the time the shake-table testing reported here was performed. Therefore, no full-scale, dynamic test data

existed that characterized natural frequencies and correlated changes in natural frequency with observed damage for CLT self-centering rocking structural systems.

The main objective of this paper is to present findings on system identification of the structure tested during Phase 1 of the UCSD-NHERI shake-table test, which corresponds to the rocking, self-centering CLT structural design solution detailed by Pei et al. (2019a). The shake-table tests were designed to progressively subject the structure to a series of historical earthquake ground motions of increasing intensity, ranging from service-level earthquake intensity to 1.20 times the maximum considered earthquake intensity. The acceleration data used to estimate the modal features were due to the low-amplitude white-noise shake-table motion tests performed immediately before and immediately after each of the earthquake shaking tests. In addition, these white-noise shake-table motions were also applied before and after each of the interventions performed.

In this paper, two output-only methods for structural identification are used, which were observed to perform well in previous tests performed on different structural systems (Moaveni et al. 2014; Belleri et al. 2014). The dynamic characterization methods are used here to systematically document the initial modal features and progressive changes to the modal parameters as damage progressed and repairs were performed during the testing program. The modal parameters estimated from the testing program are also compared with a linear finite-element model that is used to validate the modal identification results and study the performance of the two system identification methods for CLT rocking structures. Lastly, the modal results provide benchmark data that can be used in future designs of CLT rocking structures, including the estimation of initial and secant stiffnesses that can be used for design-basis earthquake (DBE) intensities.

Materials and Methods

Test Specimen Description

A 2-story structure with CLT rocking walls was tested at the UCSD-NHERI shake-table facility in 2017. Fig. 1 shows the structure on the shake table following erection. The 2-story CLT building had a rectangular planar geometry of $17,680 \times 6,100$ mm. The total height of the structure was 6,790 mm.

Glued-laminated timber (GLT) beams and columns supported gravity loads collected from the CLT floor and roof. The columns were attached to the steel base with slotted pin connections to allow for compatibility of movements due to seismic loading without introducing additional lateral loading on the columns, which mainly carry gravity loads. Two columns sizes were used: (1) GLT 273 × 190 mm, located along Gridlines A2 and A3, and (2) GLT 222 × 190 mm, located along Gridlines A1 and A4 (Fig. 2).

Two different floor systems were used on the floor and roof levels. On the floor level, primary beams had cross-section dimensions of 495 × 222 mm and spanned in the north-south (NS) direction, secondary beams had cross-section dimensions of 495 × 171 mm and spanned in the east-west (EW) direction, and the floor consisted of three-ply CLT spanning in the NS direction [Fig. 2(b)]. The roof floor system consisted of beams with cross-section dimensions of 457 × 222 mm (lateral bays) and 381 × 222 mm (central bay) spanning in the NS direction; no beams were detailed in the EW direction. The roof-level floor spanned in the EW direction and was constructed using a five-ply CLT-concrete composite system (Higgins et al. 2017), in which the reinforced concrete was 57 mm thick. Two glulam grades were specified for the



Fig. 1. Two-story CLT rocking wall structure.

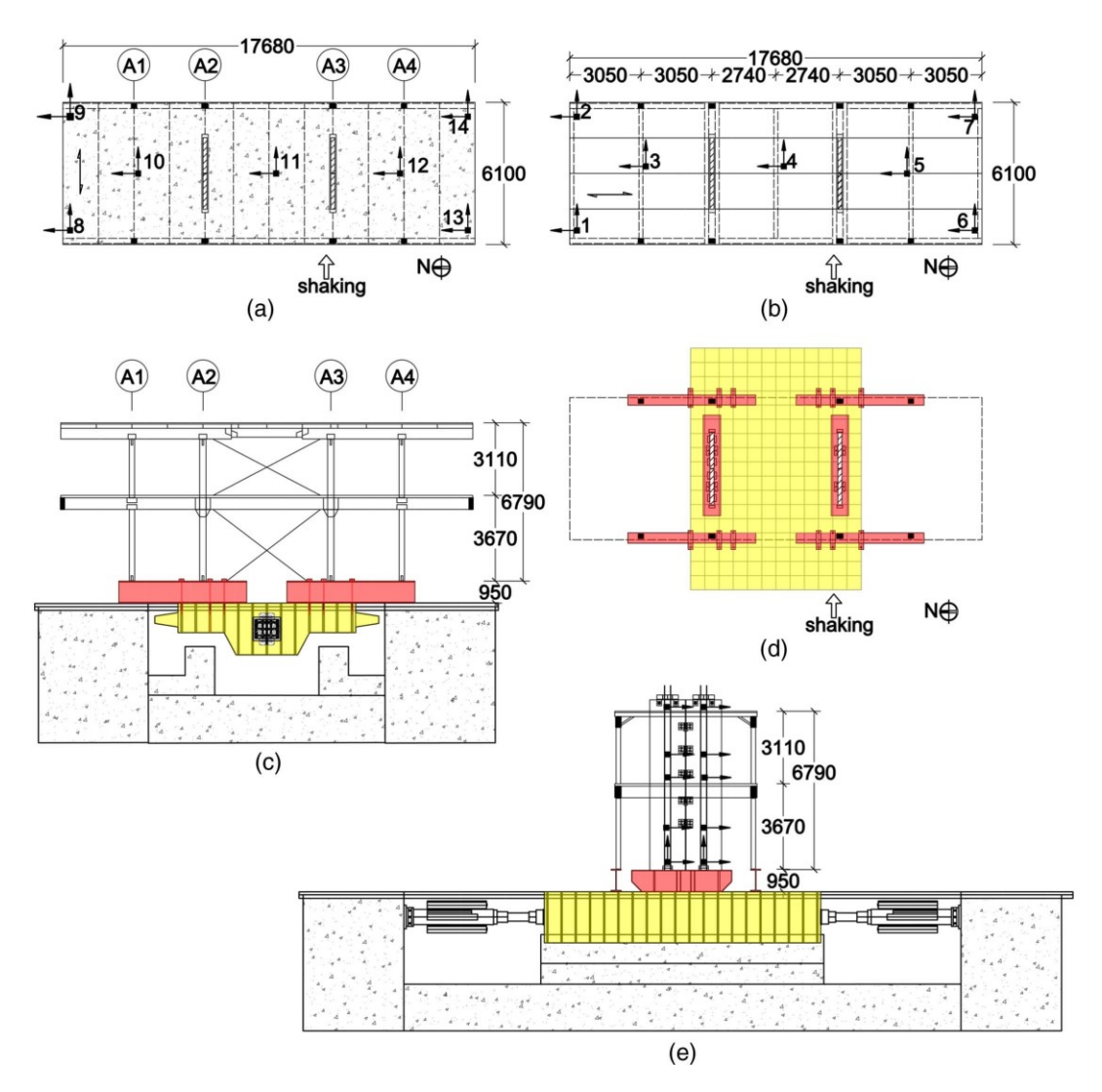


Fig. 2. CLT self-centering rocking wall test specimen: (a) roof plan view; (b) floor plan view; (c) EW elevation view; (d) foundation beam and shake-table plan view; and (e) NS elevation view. Accelerometers are marked as square boxes with arrows indicating the direction of recording. Dimensions are presented in millimeters.

gravity-resisting system of the structure: (1) grade L2 for the glulam columns, and (2) 24F-V8 for the glulam beams (American Wood Council 2015). All CLT floor members were graded V1 (ANSI/APA 2018) and made of Douglas fir (DF), *Pseudotsuga menziesii*.

The connections and elements of the CLT walls and surrounding members were designed to allow rocking and prevent sliding of walls at the base. Such connections and elements included (1) posttensioning steel bars along the full-height of the CLT walls [Fig. 3(a)], (2) steel tongue plates between diaphragms and the rocking walls [Fig. 3(b)], and (3) U-flexural plates (UFP) installed between adjacent CLT wall panels and distributed along the height of the walls [Fig. 3(c)]. The structure had two walls that consisted of two five-ply E1 panels that were 1,520 mm long connected structurally using five UFP devices. The lowest UFP was located 1,980 mm from the base of the wall, and the spacing between the five UFP devices was 960, 1,140, 1,140, and 990 mm measured from the UFP that was closest to the foundation. Each CLT panel was post-tensioned using four 19.05-mm-diameter high-strength rods [ASTM A449 Type 1 (ASTM 2020)] with a yield stress of 634 MPa.

An initial tension force of 53.3 kN was applied to each of the post-tensioning bars at the top of the wall. The walls were connected to the floors using a vertical slot tongue plate shear key, which coupled the horizontal in-plane displacements of the floor diaphragm and wall. Additional steel angles with Teflon polytetrafluorethylene sliding faces were used to provide out-of-plane displacement restraint to the wall from the floor. At the floor level, the tongue plate had a cross section of 44.5×76 mm, and at the roof level, the tongue plate had a cross section of 22×76 mm. This connection allowed only horizontal forces to be transferred between the floor diaphragms, thereby allowing walls to rock and lift without providing additional vertical restraints to the wall movement.

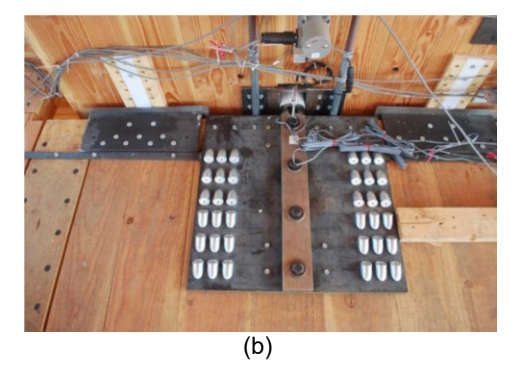
In order to stabilize the structure in the direction perpendicular to shaking and avoid excessive torsional movements, cross-bracing steel bars were added to the structure on the east and west faces between Grids A2 and A3 [Figs. 1 and 2(c)]. The cross-braces were 19-mm fully threaded rods tying the roof and second floor to the shake table's floor beams. Additional construction drawings are available for download in DesignSafe-CI (Pei et al. 2019b). The uplift of the foundation was prevented by anchoring post-tensioned rods from the top of the steel base beam to the bottom of the shake-table platform.

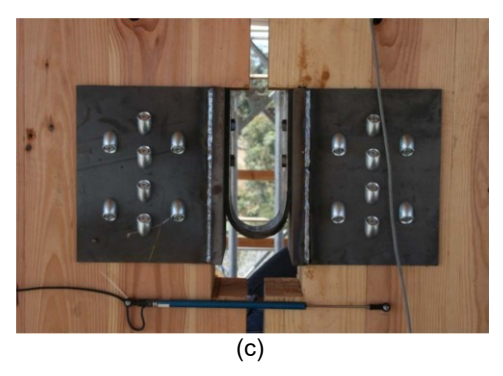
Experimental Setup, Testing Sequence, and Instrumentation

At the time of testing, the shake table was a unidirectional shaking platform with a total movement range of 7750 mm, and a peak acceleration capacity of 1.2g when loaded at a 400-t payload. The shake table was capable of producing shaking in a frequency range up to 30 Hz. The CLT structure was subjected to 14 input acceleration time series, based on four historical ground motion records: (1) 1994 Northridge earthquake, Canoga Park, (2) 1989 Loma Prieta earthquake, Capitola, (3) 1987 Superstition Hills earthquake, Poe Road, and (4) 1979 Imperial Valley earthquake, Delta. The ground motions were scaled to three seismic hazard levels considered in the building design, including the service-level earthquake (SLE), DBE, and maximum considered earthquake (MCE). The SLE, DBE, and MCE intensities considered correspond to levels used in the design of the prototype building, which was designed for a site in Oakland, California, and soil site Class B. Additional details on the design of the prototype structure have



(a)







(d)

Fig. 3. CLT rocking wall test specimen: (a) CLT wall section showing a UFP connection and four post-tensioning rods; (b) diaphragm-to-rocking wall tongue plate connection; (c) close-up of a UFP connection; and (d) close-up of a column base connection. Bolts went through slotted holes in the column. Dimensions and other detail for this connection have been reported in construction structural drawings publicly available from Pei et al. (2019b).

been provided by Pei et al. (2019a). Fig. 4 summarizes the test sequence of the input ground motions. The recorded actual shake-table motions were used throughout this study. The measured PGAs experienced by the tested structure are shown in Fig. 4 over the different input motions.

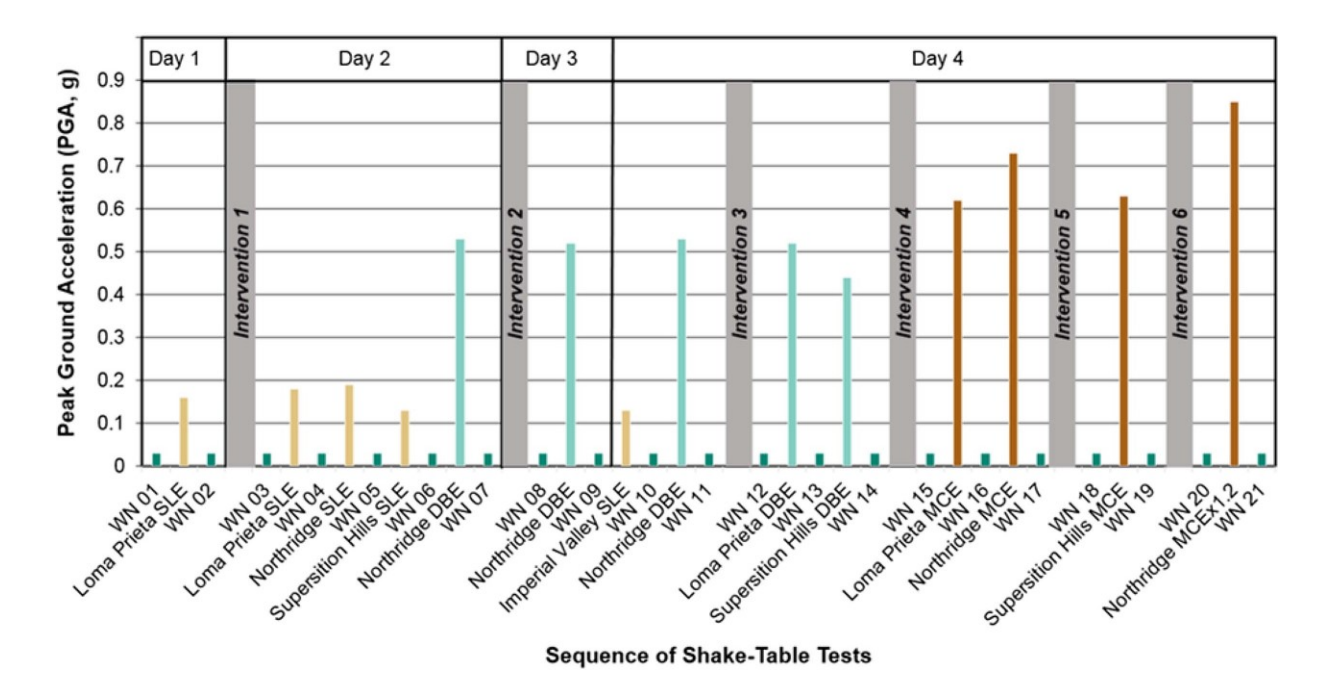


Fig. 4. Ground-motion testing sequence.

To understand the effects of damage (visible or not) to the structure from the increased shaking intensity, white-noise (WN) tests were carried out before and after each ground-motion test. In addition to the WN tests after ground-motion events, additional WN tests followed six Interventions conducted included preemptive repair or retrofitting measures, which were conducted over the test sequence. Thus, a total of 21 WN tests were conducted during the testing sequence. The WN signals consisted of a root-mean squared (RMS) acceleration of 0.03g for a duration of approximately 120 s, except for the first three WN tests, which were conducted for 240 s. Data from these WN tests are available for download in DesignSafe-CI (Pei et al. 2019b).

Six preemptive interventions were undertaken over the test sequence to make minor repairs or adjustments to the test structure that allow it to perform as intended in the structural design. In the interventions, the following actions were carried out:

- Intervention 1: The intervention taken between shake-table Tests 1 and 2 consisted of modification to the tongue plate connections (a Teflon polytetrafluorethylene interface was added) to reduce friction between the CLT wall slot and the tongue plates connected to the floor diaphragm. The Teflon polytetrafluorethylene plates were effective in reducing the friction. However, the design of the fixture of the Teflon polytetrafluorethylene plate could be improved in future designs because they tended to start to roll out of their original locations, which required that modifications and replacements had to be performed during several of the interventions. Fig. 5(b) shows a damaged Teflon polytetrafluorethylene plate (foreground) after being removed and replaced by with new Teflon polytetrafluorethylene plates (background).
- Intervention 2: This intervention took place between shake-table Tests 5 and 6, and consisted of stiffening (bracing laterally) the base beam after notable base beam deformations were observed [Fig. 5(a)].
- Intervention 3: The intervention occurred between shake-table Tests 8 and 9 whereby the post-tensioning bars were retensioned to their intended initial tension [the retension was triggered

- when there is post-tensioning (PT) force loss over 4.5 kN (1 kip)].
- Intervention 4: The intervention occurred between shake-table Tests 10 and 11, and consisted of cross-bracing retightening.
- Intervention 5: The intervention occurred between shake-table Tests 12 and 13 and consisted of cross-bracing retightening.
- Intervention 6: The intervention occurred between groundmotion Tests 13 and 14, whereby the post-tensioning bars were again retensioned to their intended initial tension and crossbracing retightened.

Microelectromechanical system (MEMS) accelerometers with a total acceleration amplitude range of T5g (g ½9.81 m=s²) were used to capture the structural dynamic response. The accelerometers were placed at seven locations on the underside of the floor and roof levels, measuring the NS and EW accelerations [Figs. 2(a and b)]. In Figs. 2(a and b), the floor-level and roof accelerometer locations are labeled 1 through 14. In addition to measuring NS and

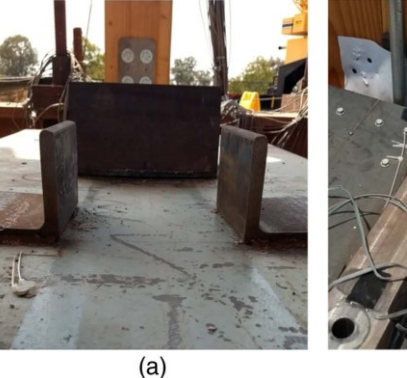




Fig. 5. (a) Base beam damage showing as downward deformation at near the middle of the top flange; and (b) replacement of the Teflon polytetrafluorethylene plates during Intervention I. (Adapted from Wichman 2018.)

EW accelerations, the accelerometers placed in the corners of the floor plans (at locations labeled 1, 2, 6, 7, 8, 9, 13, and 14) also captured vertical accelerations. One accelerometer was placed at the top of the CLT-concrete roof diaphragm to compare acceleration values with the accelerometers at Location 11 placed on the underside of the roof CLT members. Ten additional accelerometers were placed on the CLT walls. For the analysis conducted in the current study, only the 14 accelerometers located on the CLT floor and roof panels are used, corresponding to a total of 36 channels (18 channels on the floor level and 18 channels on the roof level). Additional instrumentation drawings are available in Design-Safe (Pei et al. 2019b).

Operational Modal Analysis and Damage Assessment Procedure

Two operational modal analysis (OMA) methods were used for analyzing the WN acceleration data, namely enhanced frequency-domain decomposition (EFDD) and the stochastic subspace identification (SSI).

The EFDD method is derived from the frequency-domain decomposition, a method in which the power spectral densities of a linear time-invariant system are performed (Brincker et al. 2001). The EFFD method decomposes the frequency content of the output data into independent single degrees of freedom acting along the frequency range of interest. A key assumption in the EFDD method is that the input data are of a white-noise type, meaning that their power spectral densities are constant. Secondly, the damping model used in the EFDD method follows the viscous damping model for linear-elastic systems. In the EFDD method, the natural frequencies and damping ratios are obtained by transforming the single-degree-of-freedom frequency data into the time domain and finally using the crossing time method and logarithmic decay approach for the natural frequencies and damping ratios, respectively.

The SSI method relies on the use of a state space model, effectively turning the second-order differential equation of motion into a first-order differential equation (Brincker and Andersen 2006). The following assumptions of the SSI method should be noted: (1) the system is a linear time-invariant type, (2) the system's response can be represented by a Gaussian stochastic process, and (3) a viscous damping model is adopted. Following the formulation of the state space model, the SSI method uses discretization to create time-lapsed series of the system output time-domain data. The time-lapsed series are used to create a model of the system by computing covariances between the future subsets of the output data to the prior subsets of the output data. The correlation phase allows for the system matrix to be obtained by regression, and subsequently allowing for the modal parameters to be obtained by eigenvalue analysis.

Extended explanations of the EFDD and the SSI methods have been given by Brincker et al. (2001) and Brincker and Andersen (2006), respectively. The uncertainty associated with the application of these methods directly to the shake table used in these experiments was summarized by Moaveni et al. (2014). The authors are aware that such differences and identification errors in damping ratio values have been observed in other studies using OMA methods (Magalhães et al. 2010; Moaveni et al. 2014). For example, multiple factors influence the identifiability of the damping ratios, including amplitude of the signal, spatial density of the measurements density of the signals, and model order selected (Moaveni

The methods used are available in ARTeMIS Modal version 5.2 (Structural Vibration Solutions 2017) modal identification software,

which was used to implement the SSI and the EFDD modal analysis methods. Of the several SSI techniques available in ARTeMIS Modal, the SSI-extended unweighted principal component (SSI-UPCX) (Mellinger et al. 2016) was used for all the SSI-obtained modal parameters. Because output-only OMA methods were used, the input excitation was not included in the analysis, although all input data are publicly available for download from Pei et al. (2019b).

Data Postprocessing

The WN acceleration data were collected at 240 Hz during the shake-table tests. However, the modal results were obtained by focusing on a frequency range that could be used to identify the first six significant horizontal modes of vibration, including the first and second modes in the NS, EW, and torsional directions. For consistency, data were organized into three sensor groups for analysis. First, Group 1 considered all floor level and roof channels, whereas Group 2 and Group 3 considered channels measuring accelerations in EW and NS directions only, respectively. Group 3, for example, was used to improve identification of the NS modal features because the NS direction is perpendicular to the shake-table shaking direction and therefore saw little to no shake-table excitation. For the modal feature extraction using both EFDD and SSI methods, the acceleration data were downsampled using a low-pass filter with an upper-frequency cutoff at 80% of the downsampled frequency. The acceleration data were downsampled to 12, 6, and 3 Hz to focus on different frequency ranges of interest based on a preliminary inspection of power spectral density results, which revealed several frequency peaks of interest below 12 Hz. After a preliminary analysis of the data, a model order of t/440 was consistently used to extract modes using the SSI method.

Finite-Element Modeling

Initial-State FE Model. A linear-elastic finite-element (FE) model of the structure was developed for the initial state of the structure before it was subjected to any strong shaking using general-purpose finite-element structural analysis software SAP2000 version 19 (CSI 2017). The FE model included seven different categories of frame and shell elements representing: (1) glulam columns, (2) glulam beams, (3) three-ply CLT diaphragm for the floor level, (4) CLT-concrete composite diaphragm, (5) five-ply CLT shear wall, (6) post-tensioning steel rods, and (7) experimental features such as steel base beams and cross-bracing. A geometric representation of the FE model is shown in Fig. 6.

Due to the orthotropic behavior of CLT, all CLT members were modeled as orthotropic thin-shell elements. Orthotropic shell modeling entailed estimating shear and elastic moduli for in-plane and out-of-plane directions. The in-plane moduli of elasticity (E_1 and E_2) along the strong and weak axes of a CLT panel were assigned based on E_0 compression tests listed by Barbosa et al. (2019) on five-ply DF ($Pseudotsuga\ menziesii$) CLT. Barbosa et al. (2019) obtained the strong-axis modulus of elasticity E_1 of five-ply DF CLT from testing of five specimens and resulted in a mean value of 9.0 GPa with a coefficient of variation equal to 3.1%. To derive the weak-axis modulus of elasticity (E_2), the composite theory (k-method) defined by Blass and Fellmoser (2004) was adopted. The k-method in-plane moduli of elasticity relationships are

$$k_3 \ 1 - 1 - \frac{\sum_{g_0}}{E_0} \cdot \frac{a_{m-2} - a_{m-4} + \cdots + Ta_1}{a_m}$$
 ð 1 b

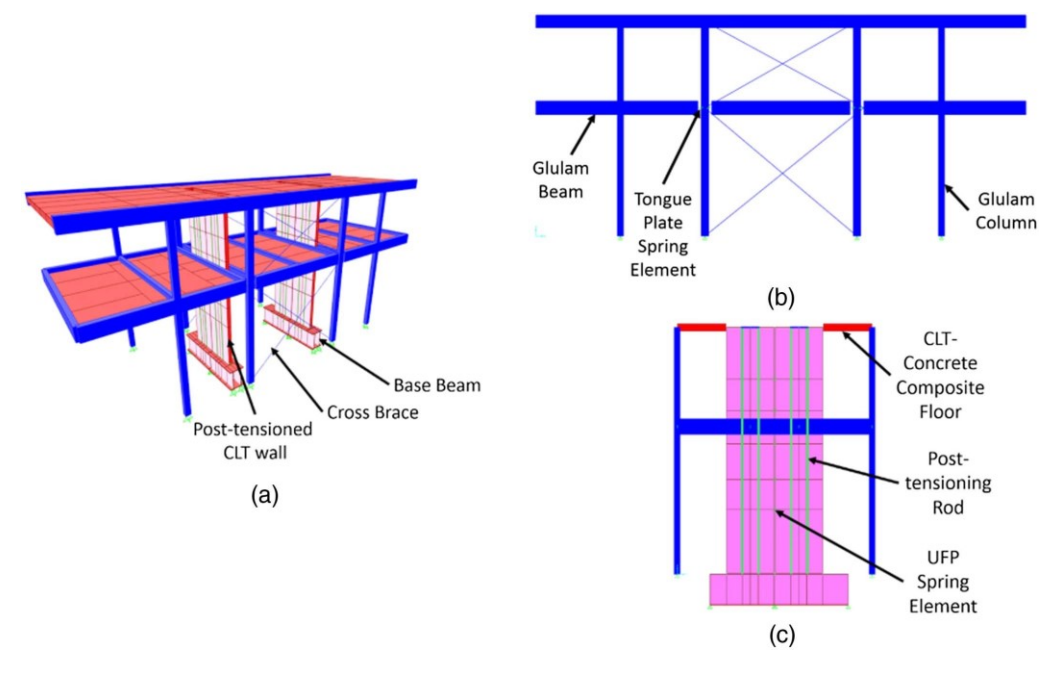


Fig. 6. Geometric representation of the FE model of the structure: (a) isometric view; (b) north-south elevation; and (c) east-west elevation.

$$k_{4} \frac{E_{90}}{E_{0}} = 1 - \frac{\sum_{E_{90}} \sum_{a_{m-2} - a_{m-4} \neq \cdots = Ta_{1}} \sum_{\delta \neq a_{m}} \frac{1}{a_{m}} \frac{1}{2} \frac{1}{$$

where k_3 and k_4 = composite factors for loading parallel and perpendicular to the strong axis of the CLT panel, respectively; a_m = total depth of the CLT panel; a_1 = thickness of the middle lamella; and a_{m-2} and a_{m-4} = thickness of the total CLT depth

subtracted by the thickness of the two and four outer lamellae, respectively. The modulus of elasticity of a single lamella in the direction perpendicular to grain, E_{90} , and its ratio to the strong axis lamellar modulus of elasticity, E_0 , E_{90} = E_0 , has been estimated to be 0.05 and 0.068 for the radial and the tangential axes for DF lumber, respectively. The CLT Handbook (Gagnon and Popovski 2011) recommends an E_{90} = E_0 ratio of 1/30, which was assumed for the computation of E_2 . The recommended values from the *CLT Hand*book were used because it is commonly adopted in the design procedures used in North America.

The in-plane shear modulus G_{12} was computed using the method developed by Bogensperger et al. (2010), given by

$$G_{1/2}^{\prime\prime} = \frac{G_{0,l;\text{mean}}}{1 \triangleright 6 \cdot \alpha_T \cdot \delta a_1 = w_l \triangleright^2}$$
 Ď2aÞ

where

$$\alpha_T \frac{\Sigma}{q} p \cdot \frac{\alpha_1^q}{w_l}$$
 Ď2 b Þ

and $G_{0,l,\text{mean}}$, a_1 , and w_l = shear modulus, average thickness, and average board width of the CLT lamellae. The parameters p and q were determined by reported values from Dröscher and Brandner (2013), and calibration from shear modulus experimental testing by Barbosa et al. (2019). In determining G_{12} , $G_{0:limean}$ was set equal to $0.0625 \times E_0$ according to estimates provided in the CLT Handbook (Gagnon and Popovski 2011). The out-of-plane stiffness properties were computed using the shear analogy method, as provided in the

CLT Handbook (Gagnon and Popovski 2011). Table 1 summarizes the material properties used in the FE model for various elements.

The tongue plates effectively acted as the boundary elements for the CLT floors, transferring load to the shear walls. The tongue plates were idealized as a rigid element with rotational springs at the diaphragm end with stiffness given by

$$\frac{3E_sI_{\mathrm{TP}}}{}_{\mathrm{TP}}K$$
 $l^{1/4}_{}_{\mathrm{TP}}$

where E_s , I_{TP} , and I_{TP} = tongue plate material modulus of elasticity, second moment of inertia about the direction perpendicular to the diaphragm floor, and the assumed length between the point of fixity of the tongue plates and wall connection, respectively. The length of the tongue plate, shown in Fig. 3(b), was 912 mm, and the tongue plate was attached to a steel wing plate using several hex bolts. The wing plate, in turn, was attached to the CLT floor using the 45° inclined screws shown in the figure. Thus, a simplified model as the one shown in Eq. 3 requires the assumption of the effective length l_{TP} , which is a function of the assumed fixity for the tongue plate and a single point of load transfer between the wall and the tongue plate. The length l_{TP} was assumed to be 304 mm,

Table 1. Summary of material properties used in this study

	N			
	Orthotropic			Isotropic
Material/members	E ₁ (GPa) E ₂	(GPa) G_{12}	(GPa)	E (GPa)
CLT, 3-ply	9.94	5.21	0.59	
CLT, 5-ply	9.00	6.16	0.64	_
Glulam beams ^a	_	_	_	12.41
Glulam columns ^a	_	_	_	11.72
Post-tensioning bars	_	_	_	196.5
All other steel members	_	_	_	200

^aFor the purpose of simplifying the FE model, glulam beams and columns were modeled as isotropic materials.

which is equivalent to the distance from the first hex bolt (closest to the wall) and the center of the wall. However, the results of some modal frequencies of the FE model are sensitive to this assumption, as discussed subsequently. Furthermore, the vertical stiffness was set to zero to capture the design features, which decoupled the horizontal motion of the diaphragm and walls from the vertical motion of the walls.

Similar to the tongue plate connections, the UFPs were modeled as spring elements. As the walls rocked, the UFPs coupled the movement of adjacent walls. Following recommendations from Baird et al. (2014), the initial stiffness of the UFPs is given by

$$K_{\text{UFP}} \frac{16E_{s}b_{u}}{27\pi} - \frac{\Sigma_{3}}{D_{u}}$$
 ŏ4Þ

where E_s , b_u , t_u , and D_u = modulus of elasticity, width, thickness, and diameter of the UFP steel plates, respectively. The UFPs in the tested structure were manufactured with a b_u value of 114 mm, t_u value of 10 mm, and D_u value of 92 mm. The Young's modulus of steel E_s was set to 200 GPa.

The last set of springs discretized the behavior of the base of the CLT wall panels in compression during rocking. Following recommendations from Akbas et al. (2017), the springs at the interface between the bottom of the CLT wall and the steel base beam are given by

$$K_{ew} \frac{1}{4} \frac{E_1 \cdot A_c}{h_c}$$
 Ď5Þ

where A_c = cross-sectional area of the compression block; and h_c = compression block height. The compression block cross-sectional area A_c was computed as the product of the thickness of the five-ply CLT panel, a_m , and the width assumed to be 3/8 of the length of the wall, L_w , at the effective elastic limit, per recommendations from Akbas et al. (2017). The compression block height h_c was assumed to be equal to 0.5 × a_m , a value that was approximately equivalent to the height of the observed CLT wall damage at the compression block locations (Pei et al. 2019a). The base of CLT wall spring elements and the post-tensioning bars acted as the boundary elements for the CLT walls.

To capture the modal response of the shake-table structure in the NS direction as well as in torsion, the steel rod cross-braces were also modeled. The steel rods had a diameter of 19 mm, consisting of A36 steel grade. Thus, the rods were assigned a Young's modulus of 200 GPa.

The base beam was observed to have affected the behavior of the structure (Pei et al. 2019a), and therefore the base beam was also included as part of the FE model. The base beam was modeled as steel shell elements of the same dimensions used in the physical experiment (the "Test Specimen Description" section gives the measurements of the base beam steel plate members). The boundary conditions of the base beams and gravity columns in the elastic model were all idealized as pinned supports to the base to replicate the low-amplitude boundary conditions of the experimental study. The post-tensioning bars were modeled as 19-mm-diameter tendons with a modulus of elasticity of 196.5 GPa.

The estimated mass of the structure included the self-weight of all structural members in addition to the added seismic weights (steel plates) that were used to represent the weight of the superimposed dead loads. All of the masses were realistically distributed according to building element locations and added seismic weights at the appropriate locations to match the experimental test conditions. The added seismic weights were 156 kN for the roof and 313 kN for the floor level (Pei et al. 2019a).

Damaged-State FE Model. Several sources of damage were identified to have occurred during the testing sequence (Pei et al. 2019a). Thus, the initial FE model described in the previous section was adjusted to incorporate the effects of damage by modifying the stiffness of various elements. The most sources of damage are summarized here in the interest of completeness and readability of the paper. The effects of damage were considered in modeling of (1) base beams, with minor residual deformations of the base beams following the first few shake-table tests, requiring the base beam to be reinforced with stiffeners, as described in Intervention 2, and (2) CLT wall corners, with minor crushing of the CLT wall panel corners at the base.

In addition to the observed structural damage, other sources affecting the frequencies of the structure were identified and adjusted. In the direction perpendicular to the shaking, the cross-braces exhibited loosening during shaking. They were retightened at several stages of the test sequence (as described previously in terms of the various interventions). Although minor damage was also observed in the column base and some beam-to-column connections, these were assumed not to have a large impact on the initial stiffness of the structure because most of these connections were designed with slotted connections to allow for displacement compatibility between the LFRS and the gravity system (Pei et al. 2019a). Thus, these were neglected for the low levels of excitation studied as part of the WN testing.

Additionally, a few CLT wall post-tensioned rods exhibited some loss of tension during the testing sequence and were subsequently retensioned to the specified design tension force, having eventually yielded and losing 30% of the initial tensioning force after 1.20 × MCE test (Pei et al. 2019a). However, when the structure was subjected to small deformations under the white-noise excitations, the post-tensioning rods provide a small contribution to the stiffness of the structure, as observed from a preliminary sensitivity study that was part of this research but not shown here in the interest of brevity. In other words, even though the steel rods were observed to yield following the 1.2 × MCE motions, up to that point, the magnitudes of the exhibited losses in post-tensioning force did not alter the white-noise-induced small vibration building frequencies significantly.

Results and Discussions

Experimental Test Results

System Identification of the Structure

The frequency peaks of the structure were initially evaluated using power spectral density (PSD) with a focus on a frequency range below 6 Hz and without data filtering. Fig. 7 displays the time series and PSDs of Channels 14E and 14N located at the southeast corner of the roof level, which measured accelerations in the EW and NS directions, respectively. The figure shows time signals and PSDs for WN tests at the start (WN 01) and the end (WN 21) of the shake-table testing sequence. It can be observed that the Channel 14E acceleration time series shows higher amplitudes compared with the Channel 14N acceleration time series, which is mainly because the shake-table shaking was in the EW direction only. The PSDs show a distinct frequency peak at 1.40 Hz for Channel 14E data. Results from Channel 14N display a less distinctive peak at 1.55 Hz. From this analysis alone, the frequency peak observed in the Channel 14N data indicates that a natural frequency from either a torsional or NS translational mode of vibration is being produced despite the shake-table shaking only in the EW direction.

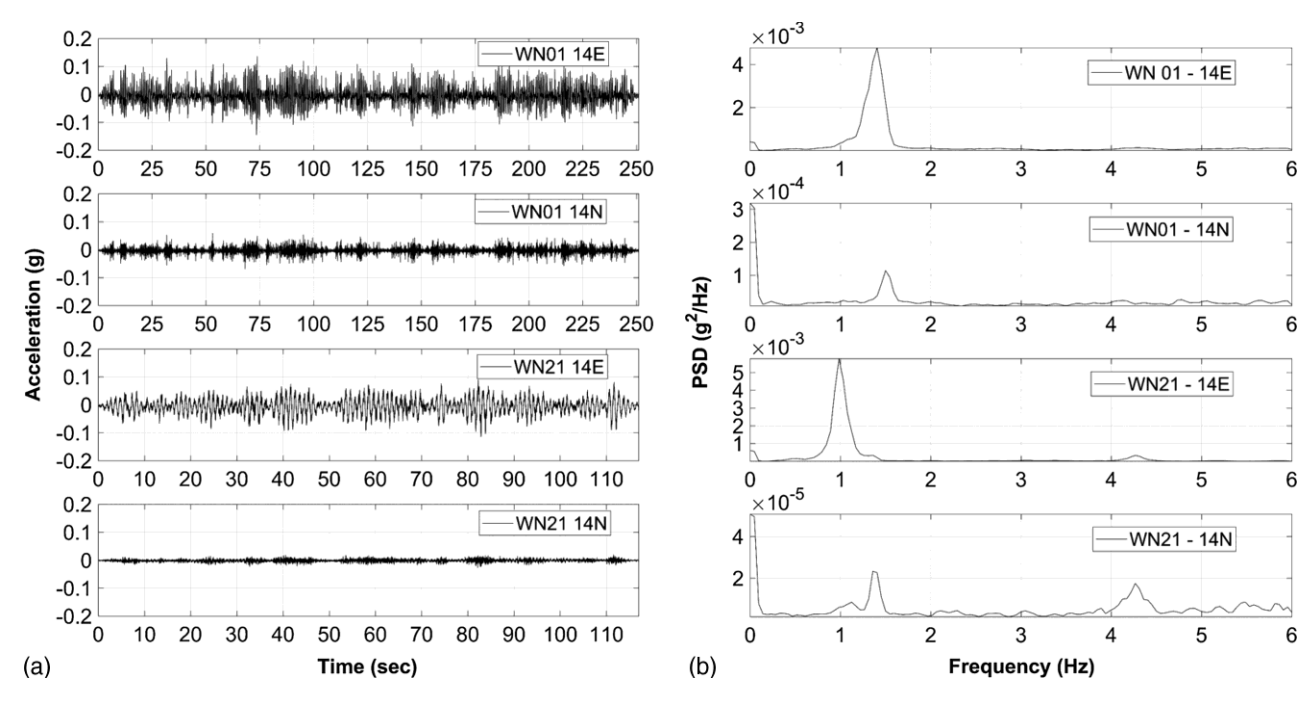


Fig. 7. White-noise time signals and power spectral densities: (a) time signals of Channels 14E and 14N for white-noise Test 1 at the start of the shake-table test sequence and white-noise Test 21 at the end of the testing sequence; and (b) power spectral densities of Channels 14E and 14N at for white-noise Test 1 and Test 21 of the shake-table test sequence.

Other peaks are also observed at approximately 4.3 Hz, as discussed in detail subsequently.

Using the SSI and EFDD methods, six modes of vibration are identified using the first WN trial (WN 01) data, which was conducted at the beginning of the shake-table testing sequence.

Table 2 summarizes the identified natural frequencies and damping ratios. Small variations between the natural frequencies identified using EFDD and SSI methods are observed, the largest of which amounts to a 3.7% difference for Mode 1. The damping ratios identified using the EFDD and SSI methods vary considerably, whereby the identified damping ratios for Mode 1 are 3.7% and 7.4% using the EFDD and SSI methods, respectively. Similarly, the damping ratios identified for Mode 4 are approximately 8.5% and 16.4% using the EFDD and SSI methods, respectively. Such variations in damping ratios have been documented and justified before in other shake-table studies (e.g., Moaveni et al. 2014) and ambient vibrations studies (e.g., Mugabo et al. 2019) when different structural identification methods are used. As can be observed from Fig. 8, vibration Mode shapes 1 and 4 are the first and second translational modes of vibration in the EW direction, Mode shapes 2 and 5 correspond to the first and second torsional

Table 2. Natural frequencies and damping ratios for the white-noise test at the start of the shake-table testing sequence

Mode		Natural frequency, $f(Hz)$		Damping ratio (%)	
number	Direction	FDD	SSI	EFDD	SSI
Mode 1	EW	1.39	1.34	3.64	7.35
Mode 2	Torsional	1.49	1.51	2.24	2.11
Mode 3	NS	1.95	1.96	3.18	1.45
Mode 4	EW	2.83	2.87	8.53	16.39
Mode 5	Torsional	4.25	4.18	3.11	4.50
Mode 6	NS	6.31	6.26	1.70	4.71

modes of vibration, and finally, Mode shapes 3 and 6 are the first and second modes in the NS direction, respectively.

Modal Features during the Shake-Table Testing Sequence Changes in the natural frequencies and damping ratios for the identified modes were evaluated at the end of each ground-motion shake-table test as well as after interventions were made. Fig. 9 shows the changes in identified natural frequencies from each of the 21 WN tests performed, as listed in Fig. 4. Results in Fig. 9 show that the natural frequency of Mode 1, f_1 , decreased by approximately 27% at the end of the testing sequence, with other modes showing smaller reductions and even slight increases, as shown in Modes 3, 4, and 6. Before Intervention 1, a decrease of 13% in f_1 was observed following the first ground-motion test (Loma Prieta SLE intensity). This initial reduction is observed in f_2, f_4 , and f_5 , although to a lesser extent. The initial reduction was not apparent for Modes 3 and 6, which were perpendicular to the direction of shaking. Interestingly, f_3 and f_6 exhibited a slight increase. The most considerable reduction of f_5 amounted to a 9% reduction following Intervention 1 (WN Test 3), during which modifications were made to tongue plates to reduce frictioninduced transfer of vertical forces.

Moderate reductions in f_1 are observed after the remainder of the SLE round motions, as shown in the graph starting with WN 02 through WN 06.

Similar to the case of SLE ground-shaking events, f_1 following DBE and MCE ground motions shows a gradual reduction of up to 20% relative to the initial natural frequency. Following the first DBE ground motion corresponding to WN 07, f_1 displayed reductions up to 25% relative to the initial frequency value. WN 08 occurred after Intervention 2, which consisted of reinforcing the base beam with steel stiffeners. The addition of steel stiffeners caused an increase in the frequency, returning it to approximately 90% of the frequency identified prior to subjecting the structure to earthquake shaking, as can be seen in Fig. 9. This demonstrates that the base beam stiffeners, added to prevent the permanent deformation under

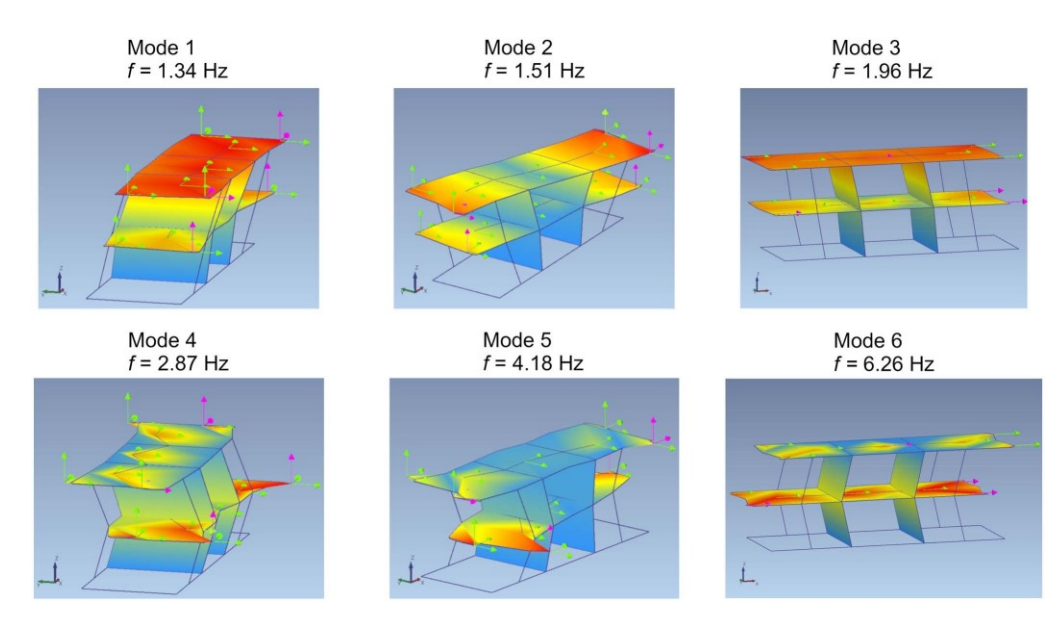


Fig. 8. Identified mode shapes and frequencies using the SSI method.

the CLT walls, resulted in stiffening the overall structural system. The increase in natural frequencies after Intervention 2 (between WN 07 and WN 08) is also observed in Mode 4 and Mode 5.

Following Intervention 2, f_4 exhibited a 46% increase, resulting in a frequency of approximately 130% of the frequency estimated at the start of the test sequence. This notable increase in frequency points to the importance of foundation effects from soil-foundation-structure interactions that can alter the dynamic behavior of a structure, in this case originating from the stiffening of the base beam. The authors were not able to conclusively pinpoint the main reason for the observed erratic changes between WN 7 and WN 11 because this was not logged during testing. Nonetheless, the data clearly indicate that changes were made at the end of Day 3, which are likely related to checking and adjusting of specimen, mainly through tightening of the transverse rods, following the public test performed on Day 3 of testing.

During WN 18, after Intervention 5, f_2 , f_3 , and f_6 experienced increases of up to 12%, 13%, and 22%, respectively. The frequency increases after Intervention 5 are only observed in the NS directions modes (f_3) and f_6 and in the first torsional mode (f_3) , demonstrating the effects of tightening the steel cross-brace rods. The steel cross-brace rods were added on the north and south center bays to reduce torsional responses in the structure during shake-table testing. The cross-braces were retightened during several of the interventions to maintain their effectiveness.

The most considerable reduction in the frequency for Mode 1 was observed following the $1.2 \times MCE$ Northridge event at the end of the testing sequence. It resulted in a 28% reduction relative to the initial frequency.

Other than Mode 1, the estimated natural frequencies of other identified modes exhibited only moderate decreases at the end of the shake-table experiment, with the second-highest reduction being 10% for Mode 2. Interestingly, at the end of the testing sequence, Modes 3 through 6 displayed natural frequencies that were equal or slightly above the frequencies estimated at the beginning of the testing sequence. This observation points toward the limited effects of damage in modes perpendicular to the direction of shaking and due to the effective retightening of the steel cross-braces over the testing sequence. The moderate changes in frequencies were also consistent with the field observations reporting only

minimal structural damage to the structure except for the interface region of the CLT walls with the base beam (Pei et al. 2019a).

The damping ratios showed substantial changes for all four identified modes throughout the testing sequence. The damping ratio associated with Mode 1 varied between 5.4% and 9.6% based on results of the EFDD analysis (diamonds) and between 3.9% and 8.6% based on the results of the SSI analysis (circles in Fig. 10). In Fig. 10, it can be seen that the damping ratio for the main EW modes (Modes 1 and 4) increases between Interventions 1 and 2, which is an opposite trend seen in the decrease of the natural frequencies. Assuming the mass is constant, the critical damping may decrease as the stiffness decreases, which is implied as the frequency decreases. Thus, the damping coefficient, i.e., the estimated viscous damping, would tend to be constant, even though the damping ratio increases due to the decrease in the critical damping. The testing and analysis cannot confirm this explicitly, and further research could be developed to answer this specific hypothesis in a controlled small-scale experiment.

More considerable differences in damping ratios were observed as a result of using the two methods of analysis. As an example, Mode 4 displayed large differences in damping ratio when extracted using the two modal analysis methods for the majority of the testing sequence. The difference is more pronounced in the first half of the testing sequence, where there is a ratio of almost four times between the damping ratios observed using the EFDD method and the ones observed using the SSI method [Fig. 10(d), WN 04]. Such differences in damping ratios are most likely due to current limitations in the estimation of damping under low excitation levels when OMA methods are used (Magalhães et al. 2010; Moaveni et al. 2014). The structure is expected to respond in a quasi-linear manner in response to the low-amplitude system identification white-noise acceleration shake-table tests performed. Thus, it is expected that the damping ratio value estimates are independent of the level of damage observed, unlike what would be expected if the base motion induced large nonlinearities, as expected during large intense ground shaking.

Finite-Element Modeling Results

Fig. 11 shows the frequencies estimated using the FE model normalized by the identified frequencies obtained using the SSI

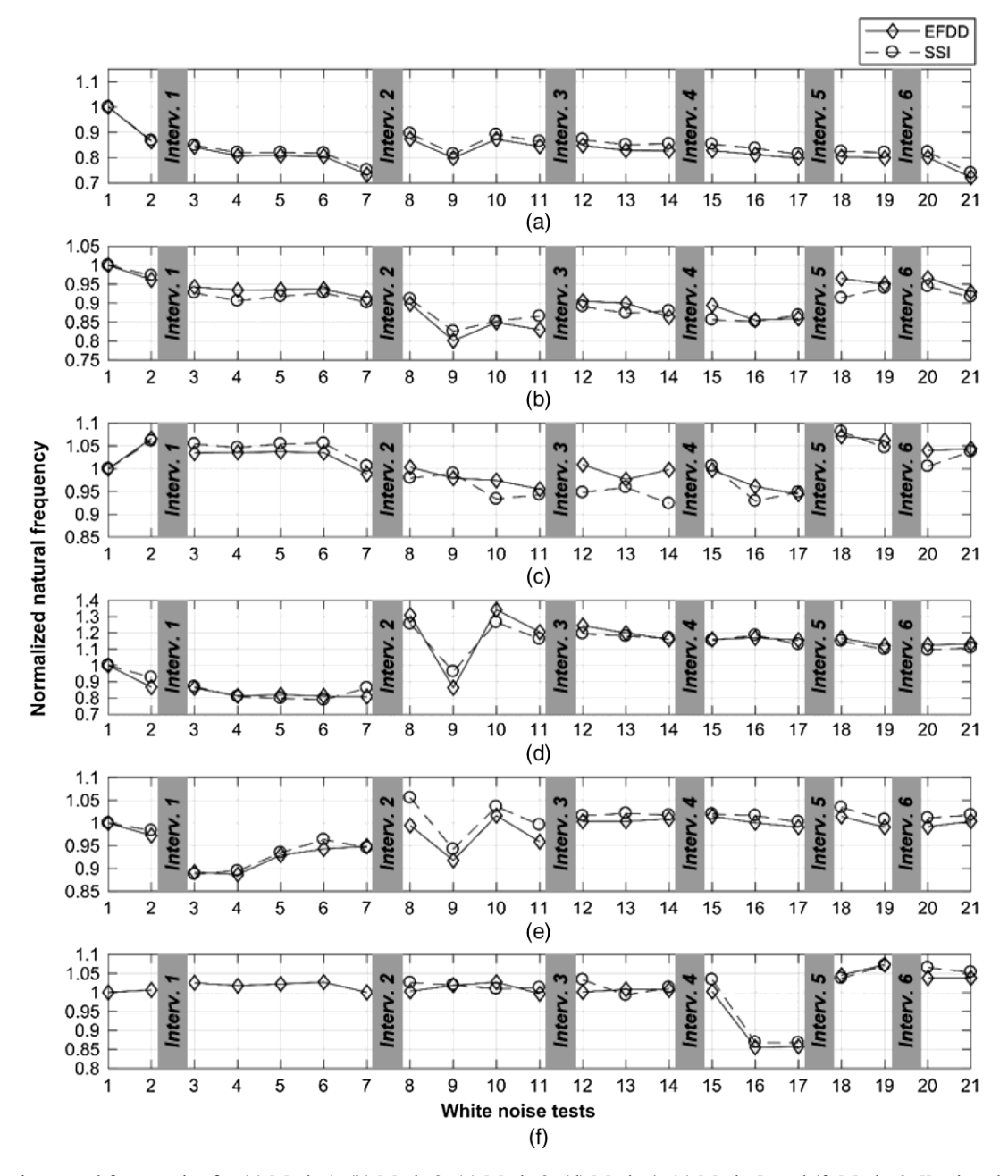


Fig. 9. Changes in natural frequencies for (a) Mode 1; (b) Mode 2; (c) Mode 3; (d) Mode 4; (e) Mode 5; and (f) Mode 6. Y-axis values are natural frequencies normalized to the natural frequencies at the beginning of the testing sequence.

method. In the interest of brevity of this paper, comparison are only made with results based on the SSI analysis. Overall, there is a good agreement in most of the FE model frequencies, except f_4 , which exhibits a 46% difference between the FE model frequencies and the SSI-identified frequencies.

In identifying reasons for the differences in f_4 , a sensitivity study of the FE model revealed that a change in the effective stiffness of the tongue plates resulted in a considerable shift in the frequencies of the nonmatching modes. At the same time, the change in effective stiffness of the tongue plates produced a small effect on other FE model modes. Although a single rotational stiffness cannot fully represent the exact mechanics of the tongue plate connections, the best match in f_4 and f_5 occurred with the use of a single rotational stiffness with an effective length of the plate equal to 304 mm, which corresponded to the distance between the first bolt of the tongue plate and the centerline of the shear wall. When

developing the elastic structural models that account for the effects of damage, four effects were considered: (1) damage to the base beam, (2) damage to the rocking wall base, (3) loosening of cross-braces, and (4) combined effects of Effects 1-3. These are detailed in the next subsections.

Damage to the Base Beam

The base beam damage was idealized by creating plastic hinges at the two edges where the top flange met the two web plates of the base beam (quasi-box beam). The plastic hinges were assumed to yield and assigned a postyield hardening modulus of elasticity of $1\% E_s$. The modeled reduction on the base beam stiffness resulted in natural frequencies that were 86% and 94% of the initial values for the EW and torsional frequencies, respectively. The stiffness reduction of the base beam did not result in a reduction in the NS fundamental frequency $(\vec{f_3})$. The lack of frequency reduction

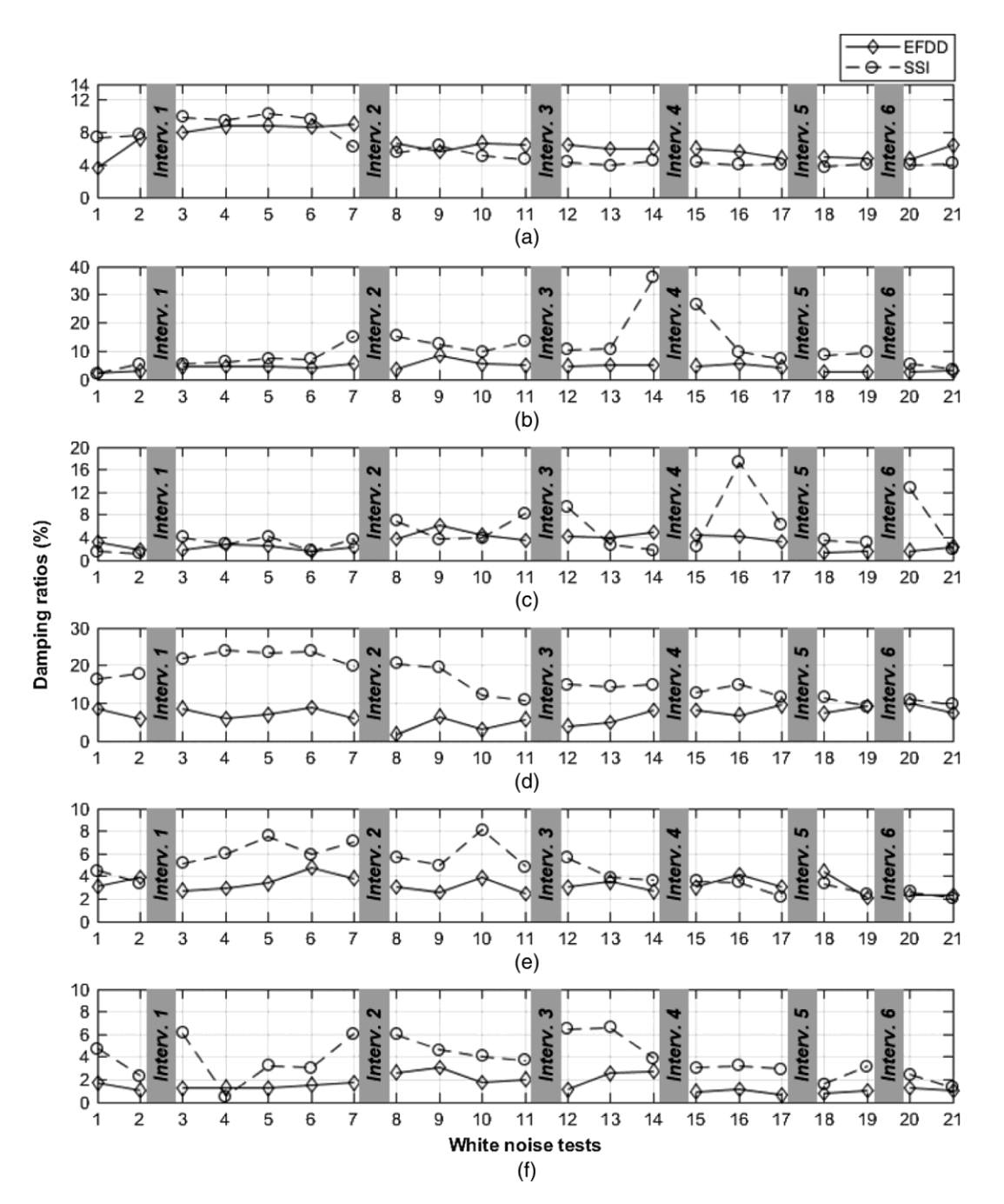


Fig. 10. Changes in damping ratios for the identified modes: (a) Mode 1; (b) Mode 2; (c) Mode 3; (d) Mode 4; (e) Mode 5; and (f) Mode 6.

for Mode 3 is consistent with the experimental results, where no reduction was observed following Intervention 2 before WN 08, when the base beam was reinforced with additional steel stiffeners. The effect of considering the damage to the base beams in terms of the natural frequencies are presented in Fig. 12 as horizontal solid lines (level 1 lines).

Damage to the Base of the Rocking Wall

The second effect considered was the stiffness reduction of the wall corner springs at the intersection between walls and the base beam. Using Eq. (5), the wall spring stiffness was computed to be approximately 5.25×10^6 kN=m. The damage observed in the wall corners included splitting, local crushing, and minor gaps between the base of the wall and base beam. These features can be modeled

as a reduction in the cross-sectional area of the compression block. As a result, a spring stiffness reduction factor of 1/20 was introduced by fitting the loss of stiffness due to crushing on five-ply CLT samples in tests conducted by Barbosa et al. (2019). The effect of this damage resulted in natural frequencies that were 84% and 93% of the experimental EW and torsional frequencies, respectively. The NS fundamental frequency exhibited a 2% reduction due to this effect. Fig. 12 shows these results as horizontal dash-dotted lines (level 2 lines).

Loosening of Cross-Braces

The third effect considered was the reduced axial stiffness of the cross-braces. The axial stiffness was considered to change by a factor of 0.25 to match the total reduction range observed

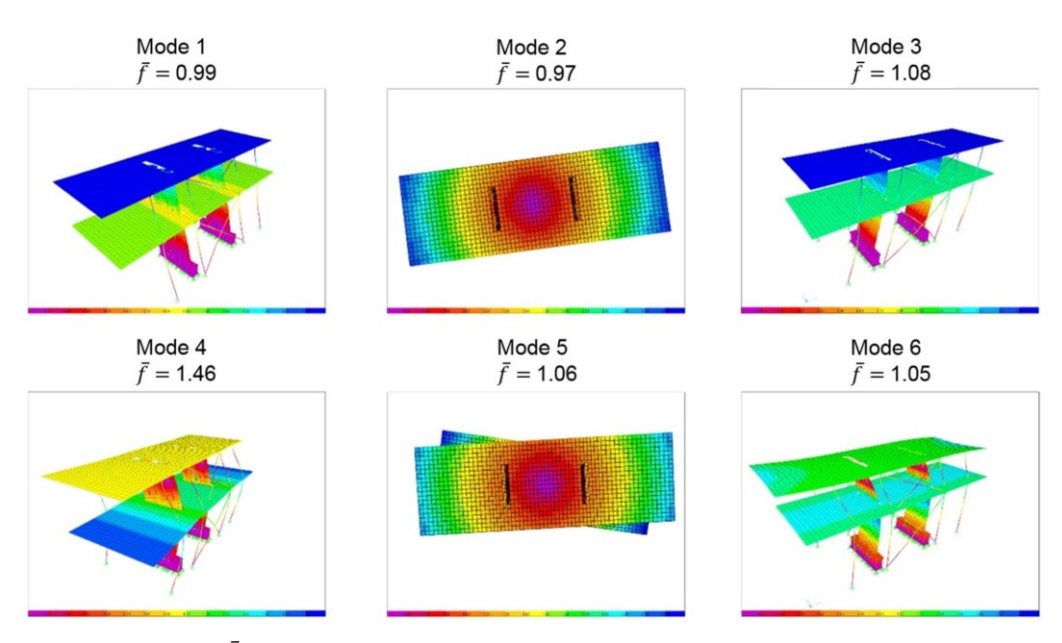


Fig. 11. FE modes shapes. The parameter represents the FE modal frequencies normalized by the corresponding modal frequencies identified using the SSI analysis (Fig. 8).

for the NS direction because damage to the base beam and the rocking walls did not affect the NS-direction frequencies. The reduction in cross-brace stiffness resulted in 93% of the experimental frequency in the NS direction. The torsional fundamental frequency

showed a reduction of up to 88% of the experimental frequency at the start of the shake-table tests. The EW fundamental frequency remained unchanged as a result of reducing the axial stiffness of the cross-braces. The effect of loosening cross-braces is shown in Fig. 12 with horizontal solid lines (level 3 lines).

Combined Damage Effects

The next and last case considered was introduced to provide an encompassing case that captures the observed damage by combining the effect of loss of stiffness due to the damage at the steel base beam and CLT wall base as well as the loosening of the cross-braces that were described previously. A modification was made to the rocking wall base damage effect by introducing a reduction factor of 1/600 (through calibration) to simulate more significant localized damage as observed at the end of the shake-table testing sequence. The combined damage effects resulted in frequencies of 75%, 84%, and 93% of the initial experimental frequencies in the EW, torsional, and NS directions, respectively. The last case combining all damage effects is presented in horizontal dashed lines (level 4 lines) in Fig. 12.

Level 1 damage is consistent to the damage to the base beam, which was partially remediated during Intervention 2. This observation explains the increase in f_1 after Intervention 2 and points to the subsequent reductions being related to the damage to the base of the wall.

Mode-Shapes Analysis and FE Validation

The modal assurance criteria (MAC) analysis (Pastor et al. 2012) was performed for all WN tests to evaluate the consistency of the experimental mode shapes and observe changes in mode shapes due to the damage in the structural system. The comparison consisted of computing MAC values between the modes identified at the beginning of the testing sequence and all subsequent WN tests.

The MAC is defined by the following equation:

$$MAC_{ab} \stackrel{1}{\cancel{4}} \frac{\eth \phi_{a}^{T} \phi_{b} }{\eth \phi_{A} \phi} \stackrel{2}{\cancel{P}} \frac{\partial \phi_{A} \phi}{\partial \phi} \stackrel{1}{\cancel{P}} \qquad \qquad \mathring{0}6P$$

where ϕ_a = mode shape a; and ϕ_b = mode shape of mode b. For the purpose of this study, the MACab is used to compare the mode shape at the beginning of the experimental testing program with the same mode shapes at several stages of the experimental tests as well as the FE mode shapes.

Fig. 13 features a selection of four MAC plots to show a comparison of experimental mode shapes taken at different stages of the testing sequence, as well as comparisons of experimental and FE model mode shapes at the start of the shake-table sequence. The experimental MAC plots shown represent the MAC values between modes identified in WN 01, at the start of the test, and modes identified in a subsequent WN test, ranging from WN 03 to WN 21 [e.g., Fig. 13(b) corresponds to MAC values between modes identified from WN 01 and WN 03 accelerations]. For all stages, Modes 1, 3, and 6 diagonal MAC values remained above 0.90 for the testing sequence. Modes 2, 4, and 5 recorded lowest diagonal MAC values of 0.8 (for WN 08), 0.76 (for WN 10), and 0.86 (for WN 15), respectively. A few notable trends were observed between changes in mode shapes and the schedule of interventions carried out during testing. Mode 2, which is the first torsional mode, displayed its lowest consistency to its initial mode shapes following Interventions 1 and 2. The MAC values between Mode shape 2 following Interventions 1 (WN 03) and 2 (WN 08) and the initial estimates for Mode shape 2, were 0.85 and 0.80, respectively.

For Mode 2, lower MAC values following these interventions point to the effect of retightening the cross-braces and making modifications to the tongue plate connections. Mode 4, being the second EW mode, displayed abrupt reductions in MAC values following Interventions 1 and 4. The corresponding diagonal MAC values dropped to 0.92 and 0.79 following Interventions 1 (WN 03) and 4 (WN15), respectively. Mode shape 4 appears to be largely influenced by the load-transfer mechanism at the tongue plate connections, which were designed to transfer lateral translational forces without transferring vertical forces or moments.

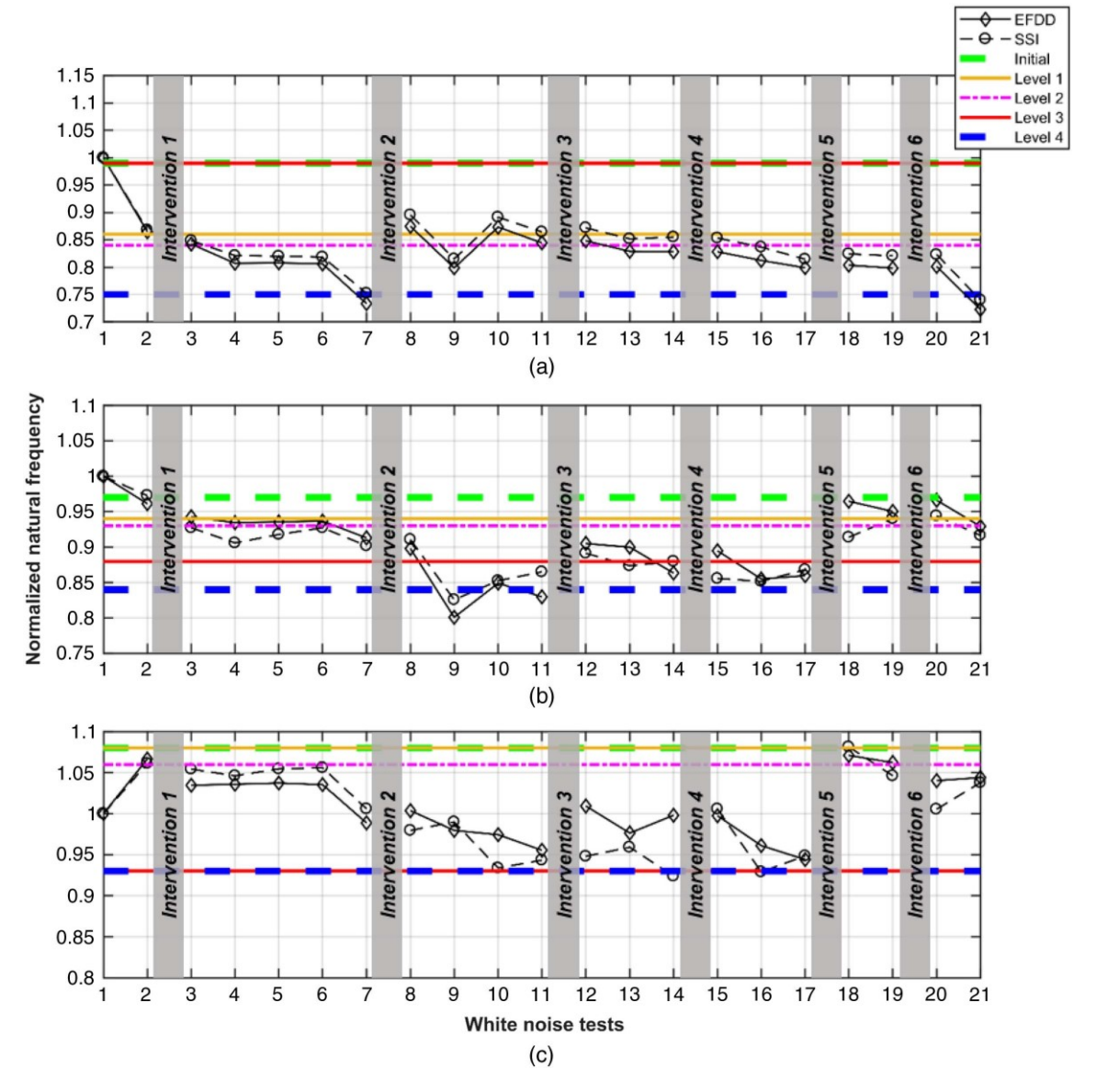


Fig. 12. Damage FE modeling for the fundamental natural frequencies: (a) Mode 1, EW direction; (b) Mode 2, torsional direction; and (c) Mode 3, NS direction. Levels 1, 2, and 3 indicate the damage to the base beam, damage to the rocking wall base, and the loosening of cross-braces, respectively. Level 4 considers the combined effects of Levels 1-3 of the damage modeling.

The observed changes in Mode shape 4 justify the modifications made to the tongue plate stiffness during the FE model calibration phase. In a similar way to Modes shapes 2 and 4, Mode shape 5 recorded the lowest MAC value following Intervention 4 (WN 15), further highlighting the influence of retightening the cross-braces and making modifications to the tongue plate connections.

The FE model mode shapes were compared with the experimental mode shapes at the start of the shake-table testing sequence. The initial FE model and the combined damage effect model mode shapes were compared with the experimental mode shapes at the beginning of the testing sequence. All diagonal MAC values between the initial experimental and the initial FE model were above 0.92, except for Mode 6, which had a diagonal MAC value of 0.88 [Fig. 13(e)]. The diagonal MAC values between the initial experimental and FE combined damage effects modes were above 0.94, except for Mode 6, which had a MAC value of 0.77. Additionally, Mode 4 of the FE combined damage effects was not detectable, most likely due to its proximity to local modes.

Conclusion

A seismic experimental program was conducted on a full-scale 2-story CLT rocking wall structure at the University of California San Diego shake-table testing facility. The shake-table program consisted of 14 ground motions of increasing intensity ranging from SLE to 1.2×MCE ground motions for a hypothetical site located in Oakland, California. In general, the 2-story CLT structure with the post-tensioned rocking walls performed well in the sense that it provided a seismic resilient design. In this study, the resiliency of the design was confirmed because there was no significant damage observed. Even though the structure was subjected to 14 intense shake-table tests, only moderate reductions (at most 28% reduction in frequency) in the fundamental natural frequency in the direction of shaking were observed.

The current study explored changes in natural frequencies and damping ratios as a result of the damage sustained as shaking intensity increased as well as features of the testing program, which

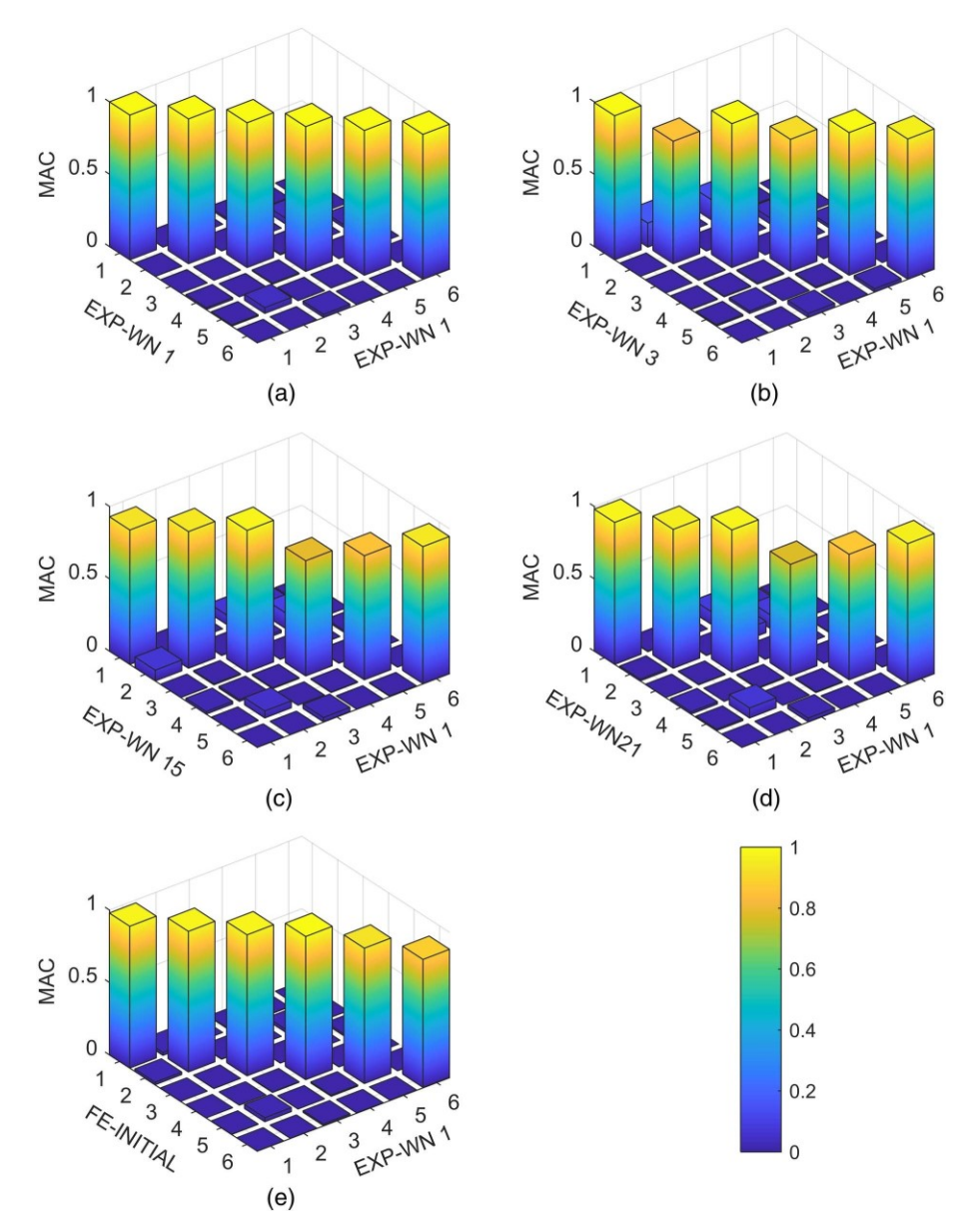


Fig. 13. MAC between experimental Modes 1-6 for WN 01 and (a) itself; (b) WN 03; (c) WN 15; (d) WN 21; and (e) the mode shapes of the FE model of the initial, undamaged structural model.

included repair and retrofits during the experimental program, in between earthquake shaking tests. The first and second modes in the NS, torsional, and EW directions were identified using two output-only methods (EFDD and SSI). The first fundamental frequency value reduced by 28% at the end of the testing program. Reduction in natural frequencies for the first five ground motions was attributed partly to the boundary conditions at the base of the CLT walls, including deformation in the steel base beam. The base beam was retrofitted with the addition of stiffeners at high CLT wall bearing force locations in the second intervention. Following this second intervention, a gradual and less abrupt reduction in the fundamental natural frequency was observed. The second natural frequency in the direction of shaking initially decreased but increased after Intervention 2 to levels above its initial value. The increase in the second natural frequency in the direction of shaking originated from the modifications made at the tongue plate connections between the CLT walls and the diaphragms.

It is well-known that the global modal features may not always detect the effects of local damage; however, results in this study illustrated the impact of damage at the base of the rocking wall structural system as well as the effect of repair and retrofit interventions performed in the tested structure.

A linear-elastic FE model was developed to capture the initial modal parameters and subsequent levels of damage consistent with the damage observed during testing. The FE model suggests that the lateral stiffness of the tongue plate connections is appreciably lower than predicted by an idealized cantilever beam stiffness. Additionally, the tongue plate stiffness has a strong influence on the second EW natural frequency due to the added flexibility at its location.

The shake-table test also provided insights into the influence of foundation-structure effects (stiffening of the base beam), retightening of the cross-braces, and modifications made to the tongue plates. The impact of each intervention could not be evaluated separately because multiple actions were done simultaneously for some of the interventions. Further research on the CLT rocking wall system is needed to determine the effects of the diaphragm to wall connections for higher modes of vibrations so that interferences

between higher modes and fundamental modes of vibrations can be avoided, especially as taller buildings with similar lateral systems and details are designed.

Data Availability Statement

Some or all data, models, or code generated or used during the study are available in a repository online in accordance with funder data retention policies (Pei et al. 2019b), or upon reasonable request to the corresponding author.

Acknowledgments

This work was financially supported by the USDA Agricultural Research Service in cooperation with the Tallwood Design Institute under Grant No. 58-0204-6-002. Additional thanks to Simpson Strong-Tie and DR Johnson for support. The National Science Foundation also supported this research project through several collaborative awards, including CMMI 1636164, CMMI 1634204, and CMMI 1634628. The use of the NHERI experimental facility is supported by the National Science Foundation's Natural Hazards Engineering Research Infrastructure (NHERI) Program. The authors would like to especially thank the NHERI at UCSD site management and staff, who helped greatly in the construction and testing program. The authors also would like to acknowledge individual industry collaborators and students who worked on this project. These include Sarah Wichman, Jace Furley, Brian DeMeza, Gabriele Tamagnone, Daniel Griesenauer, Ethan Judy, Steven Kordziel, Aleesha Busch, Ali Hansan, Joycelyn Ng, Monica Liu, and Ata Mohseni. The opinions presented herein are solely those of the authors.

References

- Akbas, T., R. Sause, J. M. Ricles, R. Ganey, J. Berman, S. Loftus, J. D. Dolan, S. Pei, J. W. van de Lindt, and H. E. Blomgren. 2017. "Analytical and experimental lateral-load response of self-centering posttensioned CLT walls." *J. Struct. Eng.* 143 (6): 04017019. https://doi.org/10.1061/(ASCE)ST.1943-541X.0001733.
- American Wood Council. 2015. National design specification (NDS) supplement: Design values for wood construction 2015 edition. Leesburg, VA: American Wood Council.
- ANSI/APA (American National Standards Institute/Engineered Wood Association). 2018. Standard for performance-rated cross-laminated timber. ANSI/APA PRG-320. Tacoma, WA: ANSI/APA.
- ASTM 2020. Standard specification for hex cap screws, bolts and studs, steel, heat treated, 120/105/90 ksi minimum tensile strength, general use. ASTM A449-14. West Conshohocken, PA: ASTM.
- Baird, A., T. Smith, A. Palermo, and S. Pampanin. 2014. "Experimental and numerical study of U-shape flexural plate (UFP) dissipaters." In Proc., New Zealand Society for Earthquake Engineering Annual Conf. Wellington, New Zealand: New Zealand Society for Earthquake Engineering.
- Barbosa, A. R., R. Soti, A. Sinha, C. Higgins, R. Zimmerman, and E. McDonnell. 2019. *In-plane shear and compression behavior of large scale cross-laminated timber panels*. Framework Project Testing Rep. Corvallis, OR: Oregon State Univ.
- Belleri, A., B. Moaveni, and J. I. Restrepo. 2014. "Damage assessment through structural identification of a three-story large-scale precast concrete structure." *Earthquake Eng. Struct. Dyn.* 43 (1): 61-76. https://doi.org/10.1002/eqe.2332.
- Blass, H. J., and P. Fellmoser. 2004. "Design of solid wood panels with cross layers." In *Proc., 8th World Conf. on Timber Engineering*. Helsinki, Finland: Finnish Association of Civil Engineers.

- Blomgren, H., S. Pei, Z. Jin, J. Powers, J. Dolan, J. van de Lindt, A. Barbosa, and D. Huang. 2019. "Full-scale shake table testing of cross-laminated timber rocking shear walls with replaceable components." J. Struct. Eng. 145 (10): 04019115. https://doi.org/10.1061 /(ASCE)ST.1943-541X.0002388.
- Bogensperger, T., T. Moosbrugger, and G. Silly. 2010. "Verification of CLT-plates under loads in plane." In *Proc., 11th World Conf. on Timber Engineering 2010*, editor by A. Ceccotti. Trentino, Italy: Trees and Timber Institute.
- Brincker, R., and P. Andersen. 2006. "Understanding stochastic subspace identification." In Proc., 24th Int. Modal Analysis Conf. (IMAC-XXIV): A Conf. and Exposition on Structural Dynamics. Society for Experimental Mechanics, 461-466. Red Hook, NY: Curran Associates.
- Brincker, R., L. Zhang, and P. Andersen. 2001. "Modal identification of output-only systems using frequency domain decomposition." *Smart Mater. Struct.* 10 (3): 441-445. https://doi.org/10.1088/0964-1726/10/3/303
- Ceccotti, A., and M. Follesa. 2006. "Seismic behaviour of multi-storey XLam buildings." In *Proc., COST Action E29 Workshop Earthquake Engineering on Timber Structures*. Coimbra, Portugal: Community Research and Development Information Service.
- Ceccotti, A., M. Follesa, M. P. Lauriola, and C. Sandhaas. 2006. "Sofie project-test results on the lateral resistance of cross-laminated wooden panels." In *Proc., 1st European Conf. on Earthquake Engineering and Seismicity*. Red Hook, NY: Curran Press.
- Ceccotti, A., C. Sandhaas, M. Okabe, M. Yasumura, C. Minowa, and N. Kawai. 2013. "SOFIE project: 3D shaking table test on a seven-storey full-scale cross-laminated timber building." *Earthquake Eng. Struct. Dyn.* 42 (13): 2003-2021. https://doi.org/10.1002/eqe.2309.
- Chen, Z., and M. Popovski. 2020a. "Material-based models for post-tensioned shear wall system with energy dissipators." Eng. Struct. 213 (Jun): 110543. https://doi.org/10.1016/j.engstruct.2020.110543.
- Chen, Z., and M. Popovski. 2020b. "Mechanics-based analytical models for balloon-type cross-laminated timber (CLT) shear walls under lateral loads." Eng. Struct. 208 (Apr): 109916. https://doi.org/10.1016/j .engstruct.2019.109916.
- Chen, Z., M. Popovski, and A. Iqbal. 2020. "Structural performance of post-tensioned CLT shear walls with energy dissipators." *J. Struct. Eng.* 146 (4): 04020035. https://doi.org/10.1061/(ASCE)ST.1943-541X .0002569.
- CSI (Computers and Structures). 2017. SAP2000: Integrated software for structural analysis and design, version 19. Berkeley, CA: CSI.
- Dröscher, J., and R. Brandner. 2013. PA13-903-1 Abschaetzung der Scheibenschubfestigkeit mit dem Pruefverfahren nach Kreuzinger und Sieder 2013. Graz, Austria: Institute of Timber Engineering and Wood Technology.
- Dujic, B., K. Strus, R. Zarnic, and A. Ceccotti. 2010. "Prediction of dynamic response of a 7-storey massive XLam wooden building tested on a shaking table." In *Proc.*, 11th WCTE World Conf. on Timber Engineering, editor A. Ceccotti. Trentino, Italy: Trees and Timber Institute.
- Gagnon, S., and M. Popovski. 2011. "Structural design of cross-laminated timber elements." In CLT handbook: Cross-laminated timber, edited by S. Gagnon and C. Pirvu. Pointe-Claire, QC, Canada: FPInnovations.
- Ganey, R., J. Berman, T. Akbas, S. Loftus, J. Daniel Dolan, R. Sause, J. Ricles, S. Pei, J. V. D. Lindt, and H. E. Blomgren. 2017. "Experimental investigation of self-centering cross-laminated timber walls." *J. Struct. Eng.* 143 (10): 04017135. https://doi.org/10.1061/(ASCE)ST .1943-541X.0001877.
- Granello, G., C. Leyder, A. Frangi, A. Palermo, and E. Chatzi. 2019. "Long-term performance assessment of an operative post-tensioned timber frame structure." *J. Struct. Eng.* 145 (5): 04019034. https://doi.org/10.1061/(ASCE)ST.1943-541X.0002308.
- Granello, G., A. Palermo, S. Pampanin, S. Pei, and J. van de Lindt. 2020. "Pres-lam buildings: State-of-the-art." *J. Struct. Eng.* 146 (6): 04020085. https://doi.org/10.1061/(ASCE)ST.1943-541X.0002603.
- Higgins, C., A. R. Barbosa, and C. Blank. 2017. Structural tests of composite concrete-cross-laminated timber floors. Corvallis, OR: Oregon State Univ.

- Holden, T., J. Restrepo, and J. B. Mander. 2003. "Seismic performance of precast reinforced and prestressed concrete walls." J. Struct. Eng. 129 (3): 286-296. https://doi.org/10.1061/(ASCE)0733-9445(2003) 129:3(286).
- Iqbal, A., S. Pampanin, A. Palermo, and A. H. Buchanan. 2015. "Performance and design of LVL walls coupled with UFP dissipaters." J. Earthquake Eng. 19 (3): 383-409. https://doi.org/10.1080/13632469.2014.987406.
- Kelly, J. M., R. I. Skinner, and A. J. Heine. 1972. "Mechanisms of energy absorption in special devices for use in earthquake resistant structures." *Bull. N. Z. Soc. Earthquake Eng.* 5 (3): 63-88.
- Kramer, A., A. R. Barbosa, and A. Sinha. 2015. "Performance of steel energy dissipators connected to cross-laminated timber wall panels subjected to tension and cyclic loading." *J. Struct. Eng.* 142 (4): E4015013. https://doi.org/10.1061/(ASCE)ST.1943-541X.0001410.
- Kurama, Y. C., S. Sritharan, R. B. Fleischman, J. I. Restrepo, R. S. Henry, N. M. Cleland, S. K. Ghosh, and P. Bonelli. 2018. "Seismic-resistant precast concrete structures: State of the art." *J. Struct. Eng.* 144 (4): 03118001. https://doi.org/10.1061/(ASCE)ST.1943-541X.0001972.
- Magalhães, F., Á. Cunha, E. Caetano, and R. Brincker. 2010. "Damping estimation using free decays and ambient vibration tests." *Mech. Syst. Signal Process.* 24 (5): 1274-1290. https://doi.org/10.1016/j.ymssp.2009.02.011.
- Mellinger, P., M. Döhler, and L. Mevel. 2016. "Variance estimation of modal parameters from output-only and input/output subspace-based system identification." *J. Sound Vib.* 379 (Sep): 1-27. https://doi.org/10.1016/j.jsv.2016.05.037.
- Milaj, K., A. Sinha, T. H. Miller, and J. A. Tokarczyk. 2017. "Environmental utility of wood substitution in commercial buildings using life-cycle analysis." Wood Fiber Sci. 49 (3): 338-358.
- Moaveni, B., A. R. Barbosa, J. P. Conte, and F. M. Hemez. 2014. "Uncertainty analysis of system identification results obtained for a seven-story building slice tested on the UCSD-NEES shake-table." Struct. Control Health Monit. 21 (4): 466-483. https://doi.org/10.1002/stc.1577.
- Mugabo, I., A. R. Barbosa, and M. Riggio. 2019. "Dynamic characterization and vibration analysis of a four-story mass timber building." *Front. Built Environ.* 5: 86. https://doi.org/10.3389/fbuil.2019.00086.
- Palermo, A., S. Pampanin, and A. Buchanan. 2006a. "Experimental investigations on LVL seismic-resistant wall and frame subassemblies." In Proc., 1st European Conf. on Earthquake Engineering and Seismology. Red Hook, NY: Curran Press.
- Palermo, A., S. Pampanin, A. Buchanan, and M. Newcombe. 2005. "Seismic design of multi-storey buildings using laminated veneer lumber (LVL)." In Proc., 2005 New Zealand Society for Earthquake Engineering Conf. Wellington, New Zealand: New Zealand Society for Earthquake Engineering.
- Palermo, A., S. Pampanin, M. Fragiacomo, A. H. Buchanan, and B. L. Deam. 2006b. "Innovative seismic solutions for multi-storey LVL timber buildings overview of the research program." In *Proc.*, 9th World Conf. on Timber Engineering WTCE 2006. Portland, OR: Oregon State University Conference Services.
- Pastor, M., M. Binda, and T. Harčarik. 2012. "Modal assurance criterion." Procedia Eng. 48: 543-548. https://doi.org/10.1016/j.proeng.2012.09.551.
- Pei, S., D. Rammer, M. Popovski, T. Williamson, P. Line, and J. W. Van De Lindt. 2016. "An overview of CLT research and implementation in North America." In *Proc.*, WCTE 2016 World Conf. on Timber Engineering. Vienna, Austria: Vienna Univ. of Technology.

- Pei, S., J. van de Lindt, A. Barbosa, J. Berman, E. McDonnell, J. Dolan, H. Blomgren, R. Zimmerman, D. Huang, and S. Wichman. 2019a. "Experimental seismic response of a resilient 2-story mass-timber building with post-tensioned rocking walls." *J. Struct. Eng.* 145 (11): 04019120. https://doi.org/10.1061/(ASCE)ST.1943-541X.0002382.
- Pei, S., J. van de Lindt, A. Barbosa, J. Dolan, and J. Berman. 2019b. Twostory wood building test. Shake table test of a two-story mass tim- ber building with post-tensioned rocking walls. Thessaloniki, Greece: DesignSafe-CI. https://doi.org/10.17603/ds2-zcb9-ry11.
- Popovski, M., J. Schneider, and M. Schweinsteiger. 2010. "Lateral load resistance of cross-laminated wood panels." In Vol. 4 of *Proc.*, 11th WCTE World Conf. on Timber Engineering, editor by A. Ceccotti, 3394-3403, Trentino, Italy: Trees and Timber Institute, National Research Council.
- Priestley, M. J. N. 1991. "Overview of PRESSS research program." *PCI J.* 36 (4): 50-57. https://doi.org/10.15554/pcij.07011991.50.57.
- Restrepo, J. I., and A. Rahman. 2007. "Seismic performance of self-centering structural walls incorporating energy dissipaters." *J. Struct. Eng.* 133 (11): 1560-1570. https://doi.org/10.1061/(ASCE)0733-9445 (2007)133:11(1560).
- Smith, T., F. Ludwig, S. Pampanin, M. Fragiacomo, A. Buchanan, B. Deam, and A. Palermo. 2007. "Seismic response of hybrid-LVL coupled walls under quasi-static and pseudo-dynamic testing." In Proc., 2007 New Zealand Society for Earthquake Engineering Conf. Wellington, New Zealand: New Zealand Society for Earthquake Engineering.
- Smith, T., S. Pampanin, A. Buchanan, and M. Fragiacomo. 2008. "Feasibility and detailing of post-tensioned timber buildings for seismic areas." In *Proc.*, 2008 New Zealand Society for Earthquake Engineering Conf. Wellington, New Zealand: New Zealand Society for Earthquake Engineering.
- Structural Vibration Solutions. 2017. "ARTeMIS modal." Accessed April 15, 2018. http://www.svibs.com/products/ARTeMIS_Modal.aspx.
- Sustersic, I., M. Fragiacomo, and B. Dujic. 2016. "Seismic analysis of cross-laminated multi-story timber buildings using code-prescribed methods: Influence of panel size, connection ductility, and schematization." J. Struct. Eng. 142 (4): E4015012. https://doi.org/10.1061 /(ASCE)ST.1943-541X.0001344.
- Tannert, T., M. Follesa, M. Fragiacomo, P. Gonzalez, H. Isoda, D. Moroder, H. Xiong, and J. van de Lindt. 2018. "Seismic design of cross-laminated timber buildings." Wood Fiber Sci. 50: 3-26. https://doi.org/10.22382/wfs-2018-037.
- van de Lindt, J., J. Furley, M. Amini, S. Pei, G. Tamagnone, A. Barbosa, D. Rammer, P. Line, M. Fragiacomo, and M. Popovski. 2019. "Experimental seismic behavior of a two-story CLT platform building." *Eng. Struct*. 183 (15): 408-422. https://doi.org/10.1016/j.engstruct.2018.12
- van de Lindt, J. W., S. Pei, S. E. Pryor, H. Shimizu, and H. Isoda. 2010. "Experimental seismic response of a full-scale six-story light-frame wood building." *J. Struct. Eng.* 136 (10): 1262-1272. https://doi.org/10.1061/(ASCE)ST.1943-541X.0000222.
- Wichman, S. 2018. "Large-scale dynamic testing of rocking cross laminated timber walls." M.Sc. thesis, Dept. of Civil and Environmental Engineering, Univ. of Washington.
- Zimmerman, R. B., and E. McDonnell. 2018. "Framework—Innovation in re-centering mass timber wall buildings." In *Proc.*, 11th US National Conf. on Earthquake Engineering. Oakland, CA: Earthquake Engineering Research Institute.